Check for updates

Efficient electromagnetic interference shielding of lightweight carbon nanotube/polyethylene composites *via* compression molding plus salt-leaching†

Ling Xu,[a] Li-Chuan Jia,[a] Ding-Xiang Yan, [ID] *[b] Peng-Gang Ren,[c] Jia-Zhuang Xu [ID] [a] and Zhong-Ming Li [ID] *[a]

Carbon nanotube/high density polyethylene (CNT/HDPE) foam composites with high electrical conductivity and electromagnetic interference (EMI) shielding performance were developed by means of compression molding plus salt-leaching. The uniform porous structure and interconnected CNT networks throughout the cell backbones endowed the as-prepared foam composites with a significantly lower electrical percolation threshold (0.22 vol%) than that of the solid composites (0.84 vol%). Owing to the multiple reflections and scattering between the cell–matrix interfaces, the foam composites presented a superior specific EMI shielding effectiveness (EMI SE) of 104.3 dB cm^3 g^{-1}, 2.2 times higher than that of their solid counterpart. Besides this, the pore sizes of the CNT/HDPE foam composites could be easily tuned by controlling the particle size of the porogen. Also, the electrical conductivity and specific EMI SE increased with an increase in the cell diameter, which was attributed to the formation of a more perfect conductive network in the cell backbones. Our approach provides a novel idea for fabricating new lightweight EMI shielding materials, especially for aircraft and spacecraft applications.

1 Introduction

Given the rapid development of electronic devices, such as communication facilities, wireless networks, portable digital hardware, *etc.*, electromagnetic pollution poses a serious problem in modern society.[1-3] Thus, electromagnetic interference (EMI) shielding materials have drawn extraordinary attention in the academic and industrial fields. Compared to traditional metal-based shielding materials, conductive polymer composites (CPCs) containing carbonous nanofillers have been viewed as advanced candidates for EMI shielding, because they are lightweight, easy to process, and resistant to corrosion, and have tunable electrical conductivity.[4-12]

On the basis of material and energy savings, being as lightweight as possible is especially important for EMI shielding materials if they are to be used in aircraft, spacecraft, automobiles, and household appliances. To this end, great efforts have

been devoted to reducing the weight of CPCs by constructing foam structures.[13-20] Unfortunately, the formation of cells inevitably impairs the conductive networks of traditionally porous CPCs, resulting in structures which hardly meet the commercial EMI shielding effectiveness (EMI SE) requirement, *i.e.*, 20 dB.[21] For instance, Yang *et al.* reported porous CPCs made of carbon nanotube (CNT)/polystyrene foam for EMI shielding that exhibited an average EMI SE of 19 dB at a density of 0.56 g cm^{-3}.[13] Ling *et al.* explored a water vapor induced phase separation process for preparing a graphene–polyetherimide foam composite with a much lower density of 0.29 g cm^{-3}. Nevertheless, an average EMI SE of only 11 dB was obtained.[22] A modified study reported an increased EMI SE of 18.2 dB by introducing ferrosoferric oxide (Fe$_3$O$_4$)-functionalized graphene, while the foam density was 0.4 g cm^{-3}.[23] Generally, raising the filler content perfects the conductive networks to improve the EMI SE of CPC foams. However, high nanofiller loading always causes adverse effects on the formation of pore structure, hindering the formation process,[23] and so, the simultaneous realization of high EMI SE and low density in CPC foams remains a daunting challenge. To solve this technical issue, our previous work proposed a facile and effective approach based on compression molding and salt-leaching to prepare graphene/polystyrene foam composites, resulting in structures with an EMI SE of 29.0 (17.3) dB with a foam density of 0.45 (0.27) g cm^{-3}, wherein the increased nanofiller loading

[a]College of Polymer Science and Engineering, State Key Laboratory of Polymer Materials Engineering, Sichuan University, Chengdu, 610065, China. E-mail: zmli@scu.edu.cn

[b]School of Aeronautics and Astronautics, Sichuan University, Chengdu 610065, China. E-mail: yandingxiang@scu.edu.cn

[c]Institute of Printing, Packaging Engineering and Digital Media Technology, Xi'an University of Technology, Xi'an, Shaanxi 710048, China

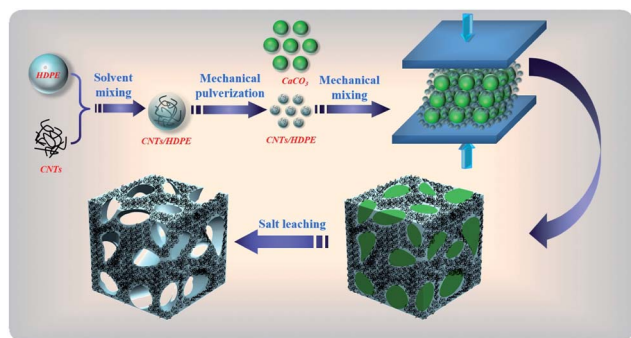† Electronic supplementary information (ESI) available. See DOI: 10.1039/c7ra13453c

Fig. 1 Schematic representation of the fabrication of the CNT/HDPE foam composites using the compression molding plus salt-leaching method.

had a slight effect on the foamability of the foam and a relatively high EMI SE and a low foam density could be achieved simultaneously.[17] Regrettably, the comparative study on the EMI shielding performance between the CPC foam and solid is still unavailable, and the contribution of the foam structure to the EMI shielding performance has not been thoroughly investigated, which is of prominent importance to guide the fabrication of efficient low density EMI shielding materials.

Herein, lightweight CNT/high-density polyethylene (HDPE) foam composites with a high EMI SE of 27.1 dB at a density of only 0.26 g cm^{-3} were easily fabricated using a compression molding plus salt-leaching technique. The resulting foam structure endowed the CNT/HDPE foam composites with a much lower electrical percolation threshold of 0.22 vol% and a significantly higher specific EMI SE (EMI SE divided by density) of 104.3 dB cm^3 g^{-1}, compared to those of its solid counterpart which were 0.84 vol% and 48.1 dB cm^3 g^{-1}. The effects of the pore size on the electrical conductivity and the EMI shielding performance of the CNT/HDPE foam composites were also investigated.

2 Experimental section

2.1 Materials

HDPE (5000S) with a density of 0.945 g cm^{-3} was purchased from Daqing petrochemical company, China. CNTs with a density of 2.1 g cm^{-3}, a diameter of 20–40 nm and a length of 50 μm were supplied by the Institute of Organic Chemistry at the Chinese Academy of Science, China. Calcium carbonate (CaCO$_3$) with a density of 2.7 g cm^{-3} was purchased from

Yibang Science and Technology Ltd., China. Three kinds of CaCO$_3$ particles were used in this work to adjust the pore sizes of the foam composites. Ethanol, hydrochloric acid, distilled water and xylene were purchased from Kelong Chemical Incorporated Co. Ltd., China.

2.2 Fabrication of CNT/HDPE foam and solid composites

The fabrication of the CNT/HDPE foam composites is schematically illustrated in Fig. 1. Initially, solution mixing and mechanical pulverization were utilized to prepare CNT filled HDPE particles. The CNT/HDPE particles were then mechanically mixed with CaCO$_3$ particles to obtain CNT/HDPE/CaCO$_3$ complex particles. Subsequently, the complex particles were compression molded into sheets under a pressure of 10 MPa and a temperature of 180 °C for 15 min. Finally, the CNT/HDPE foam composites were obtained by leaching CaCO$_3$ out of the sheets using hydrochloric acid (HCl, 10 vol%) and distilled water. The CaCO$_3$ content was fixed at 90 wt% in the CNT/HDPE/CaCO$_3$ sheets. The CNT content in the CNT/HDPE foam composites was 2, 3, 5, 10, 15, and 30 wt%. Detailed information on the CNT/HDPE foam composites is listed in Table 1. For comparison, CNT/HDPE solid composites with the same CNT content were also prepared.

2.3 Characterization

The morphologies of the foam structures were observed using field-emission scanning electron microscopy (FE-SEM, Inspect-F, FEI, USA) at an accelerating voltage of 20 kV after sputter-coating the specimens with gold. The density of the foam composites was calculated by measuring the weight and apparent volume of the samples. The average density value was evaluated using at least five samples. The electrical conductivities of the composite samples were measured using a Keithley electrometer Model 4200-SCS according to a two-point method. The EMI SE measurements were conducted using an Agilent N5230 vector network analyzer at room temperature, in the frequency range of 8.2–12.4 GHz (X band). Detailed information for the EMI shielding measurements is available in our previous work.[24]

3 Results and discussion

The microscopic morphologies of the CNT/HDPE foam composites with various CNT content are shown in Fig. 2, exhibiting typically open-cell structures in the systems

Table 1 Density, continuity of the CaCO$_3$, porosity, weight content, and volume fraction of the CNTs in the CNT/HDPE foam composites

CNT content in the solids (wt%)	CNT content in the solids (vol%)	Density of the solids (g cm^{-3})	CNT content in the foams (vol%)	Density of the foams (g cm^{-3})	Continuity of the CaCO$_3$ (%)	Porosity (%)
0	0	0.95	0	0.26	98.5	74.8
2	0.91	0.96	0.22	0.26	98.6	75.0
3	1.27	0.96	0.33	0.25	99.8	75.3
5	2.31	0.97	0.55	0.25	99.8	75.5
10	4.76	1.00	1.10	0.25	99.0	76.2
15	7.36	1.03	1.66	0.25	99.0	76.7
30	16.17	1.13	3.39	0.26	99.1	78.3

regardless of the CNT content. The evolution of such open-cell structures is attributed to the compression molding and salt-leaching method. During the compression molding process, melted CNT/HDPE particles mutually adhere to form a continuous phase in the CNT/HDPE/CaCO$_3$ sheets. The salt-leaching process dissolves the CaCO$_3$, leading to the formation of an open-cell structure with CNT/HDPE as the skeleton. The gravimetric data for the CaCO$_3$ continuity in the CNT/HDPE foam composites are above 98.5%, demonstrating that almost all of the CaCO$_3$ is removed during the salt-leaching process. As a result, the density of the foam composites is as low as ~0.26 g cm^{-3} (Table 1). The magnified SEM images in Fig. 2a$_1$–d$_1$ reveal that the CNTs are homogeneously dispersed in the cell skeletons without obvious agglomeration, which is similar to

the CNT distribution in the solid composite (Fig. S1†), and the dispersed CNTs become denser as the CNT content increases. When the CNT content is 3.39 vol%, thickly dotted CNTs are observed to construct perfect conductive networks, which engender the foam composite with excellent electrical conductivity and EMI shielding performance. The strategy proposed here is obviously superior to other molding methods, such as phase separation, supercritical carbon dioxide foaming, and other methods,[25–31] for preparing low-density foam composites with a high nanofiller content.

Fig. 3 shows the electrical conductivity as a function of CNT volume fraction in the CNT/HDPE foam composites. For comparison, the electrical conductivity of the CNT/HDPE solid composites is also displayed. A typical percolation behavior is
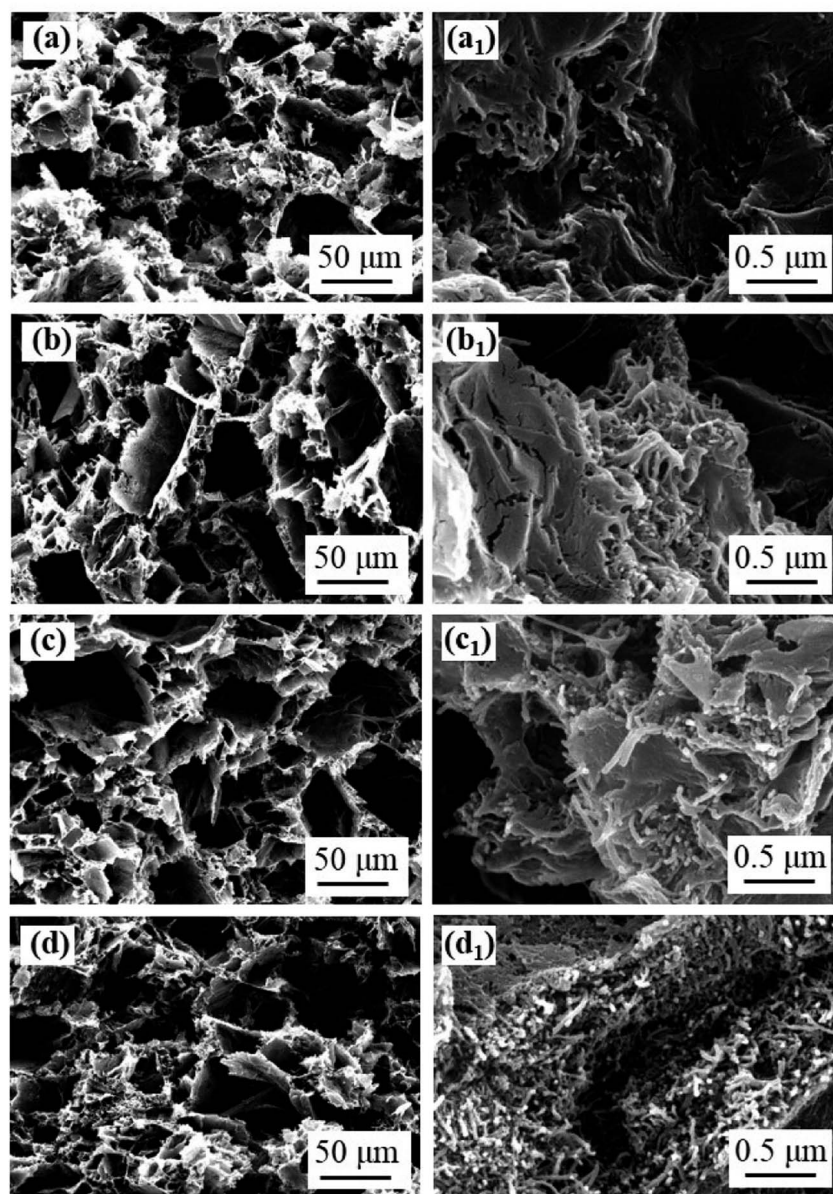

Fig. 2 SEM micrographs of the CNT/HDPE foam composites with different CNT content: (a, a$_1$) 0.33 vol%, (b, b$_1$) 0.55 vol%, (c, c$_1$) 1.10 vol%, and (d, d$_1$) 3.39 vol%.
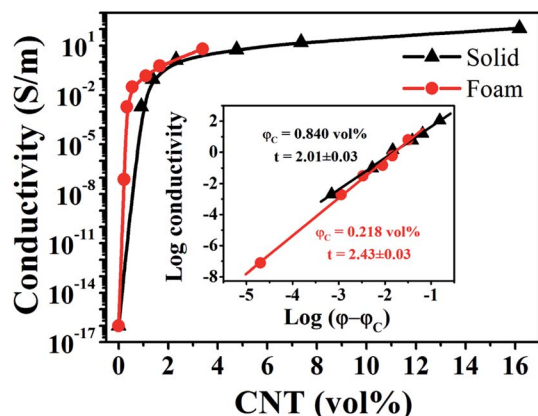
Fig. 3 Electrical conductivity *versus* the CNT volume fraction for the CNT/HDPE foam and solid composites. The inset shows the linear fitting of the data according to the power law equation.

observed for the two composites and the foam composites always exhibit much higher conductivities than their solid counterparts. For instance, the electrical conductivity of the foam composite with only 0.55 vol% CNTs is 3.2×10^{-2} S m^{-1}, more than one order of magnitude over that of the solid composite with a higher CNT content (2.06×10^{-3} S m^{-1}@0.91 vol%). The relationship between the electrical conductivity and the CNT volume fraction is influenced by classical percolation theory $\sigma = \sigma_0(\varphi - \varphi_c)^t$, where σ stands for the electrical conductivity of the composites; σ_0 is a constant related to the inherent electrical conductivity of the CNTs; φ represents the volume fraction of the CNTs; φ_c is the percolation threshold; and t is the critical index related to the dimension of the conductive networks. The inset in Fig. 3 shows good linear fitting for both the CNT/HDPE foam and solid composites according to the power law equation. The foam composites have a much lower φ_c value (0.218 vol%) than that of the solid composites (0.840 vol%). The fitted t values are 2.43 and 2.01, indicating the formation of three dimensional conductive networks in both systems.[32–34] In comparison to the solid composites, the superior electrical conductivity for the foam composites originates from their unique foam structure, which allows a concentrated amount of CNTs to distribute in the cell

skeleton, thus improving the effective CNT concentration in the whole system.

It is well known that EMI shielding performance is closely related to electrical conductivity.[35,36] The higher electrical conductivity of the CNT/HDPE foam composites is expected to be beneficial for the EMI shielding performance. Fig. 4 shows the EMI SE of the CNT/HDPE foam and solid composites. The EMI SE of both the foam and solid composites exhibits a weak dependence on frequency and this increases with CNT content. As expected, the EMI SE of the foam composites is higher than that of the solid composites at a given CNT content, in accordance with the electrical conductivity results (Fig. 3). The CNT/HDPE foam composite displays a satisfactory EMI SE 21.2 dB with only 1.66 vol% CNT content, which meets the target requirement for commercial application (20 dB), whereas a higher CNT content (2.31 vol%) is required for the solid composites. Upon increasing the CNT content to 3.39 vol%, the CNT/HDPE foam composite realizes an impressive EMI SE of 27.1 dB, which is superior to those reported in most of the previous work (Table S1†).[17,37–43] On the one hand, the excluded volume effect caused by the foam structure can drive randomly distributed CNTs to the cell skeleton and thus promote the construction of more perfect conductive networks. On the other hand, the existence of numerous interfaces between the cell skeleton and cells enhances the multi-reflection and absorption of the electromagnetic waves. The abovementioned effects are conducive to improving the EMI SE of the CNT/HDPE foam composites.

In the evaluation of the EMI shielding effect of a CPC, the weight content of the electrical filler is also considered in some cases. Fig. 5a shows the average EMI SE of the CNT/HDPE foam and solid composites with CNT weight content. At the same CNT content, the foam composites exhibit a lower EMI SE than the solid composites. This phenomenon is mainly ascribed to the dramatic reduction of effective ingredients, blocking electromagnetic waves by introducing cells in the CNT/HDPE foam composites. Note that the effective thickness of the foam composites interacting with the electromagnetic waves is only 0.58 mm, significantly smaller than that for the solid composites (2.5 mm). Therefore, the specific EMI SE (EMI SE divided by material density) is more appropriate to compare the shielding
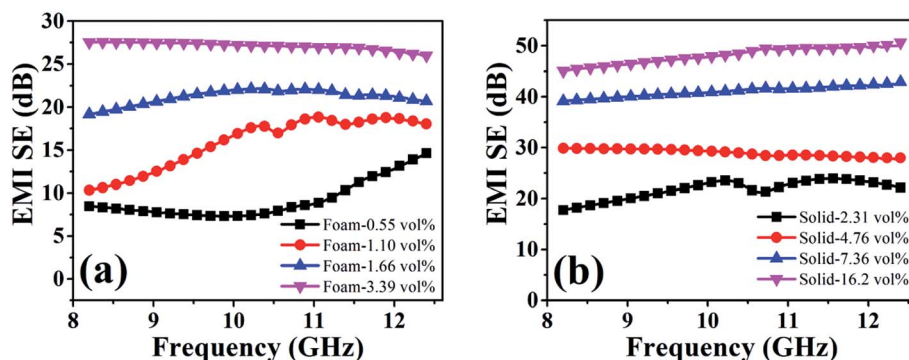

Fig. 4 EMI SE as a function of frequency in the X-band range for the CNT/HDPE foam composites (a) and solid composites (b) with different CNT volume fractions.
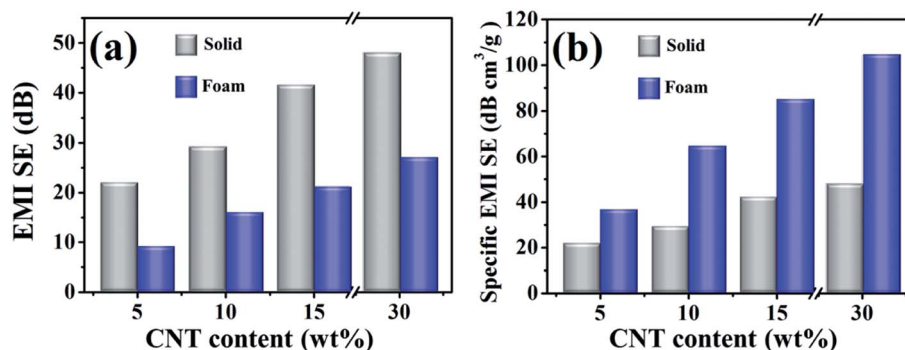
Fig. 5 The average EMI SE (a) and specific EMI SE (b) of the CNT/HDPE foam and solid composites with CNT weight content.

performance of the foam and solid composites, as proposed by Gupta *et al.*[13] Fig. 5b shows that the average specific EMI SE of the CNT/HDPE foam composites is 1.7–2.2 times that of the solid composites, showing their superior EMI shielding performance once again.

Aside from superior EMI shielding performance, the CNT/HDPE foam composites also exhibit stronger microwave absorption. Fig. 6 shows the power reflectivity (R) and absorptivity (A) of the CNT/HDPE foam and solid composites with 30 wt% and 15 wt% CNT content. It is observed that the foam composites show a lower R value but a higher A value in comparison to the solid composites. For instance, at a frequency of 8.2 GHz, the values of R (A) are ~17.0% (81.8%) and ~35.0% (64.8%) for the foam composites with 15 and 30 wt% CNT content, respectively, while the corresponding values are ~54.8% (45.2%) and ~66.9% (33.1%) for the solid composites. It is well known that the addition of CNTs enhances the dielectric constant of CPCs and intensifies the impedance mismatch between the CPC and air, resulting in increased electromagnetic wave reflection at the CPC surface. Fortunately, the integration of cells into the CNT/HDPE foam composites significantly relieves the impedance mismatch, which is conducive to reducing the wave reflection.[44] The low power reflectivity and higher absorptivity in combination with the high EMI SE enable the CNT/HDPE foam composites to be used for potential applications in the field of microwave absorption.

The relationship between the EMI shielding performance and the pore size in the CNT/HDPE foam composites was also

investigated. At a fixed foam density of 0.26 g cm^{-3} and a CNT content of 30 wt%, CNT/HDPE foam composites with three kinds of pore sizes were fabricated and their morphological observations are shown in Fig. 7. The pore size gradually decreases with a decrease in the particle size, as shown in Fig. 7a–c. The corresponding foam composites are labeled as L-CNT/HDPE, M-CNT/HDPE, and S-CNT/HDPE, respectively.

Fig. 8 shows the EMI SE of L-CNT/HDPE, M-CNT/HDPE, and S-CNT/HDPE. It can be seen that the EMI SE of L-CNT/HDPE and M-CNT/HDPE is almost independent of the frequency, while the EMI SE of S-CNT/HDPE strongly interacts with the frequency, especially at high frequencies. As the pore size reduces, the average EMI SE values are 27.1, 20.2, and 13.9 dB for L-CNT/HDPE, M-CNT/HDPE, and S-CNT/HDPE, respectively. As shown in the inset of Fig. 8, the CaCO$_3$ particles are assumed to be ideal spheres with a radius of r and the CNT/HDPE layers are uniformly coated on the CaCO$_3$ surface with a thickness of h. The relationship between h and r can be expressed by the following equation:

$$\frac{h}{r} = \sqrt[3]{\frac{V_h}{V_r} + 1} - 1$$

where V_h and V_r are the volume fractions of CNT/HDPE and CaCO$_3$ (or cells). Since V_h/V_r is consistent for the three types of CNT/HDPE/CaCO$_3$ sheets, h is proportional to r. During the compression molding and salt-leaching process, the CNT/HDPE layers evolve into a continuous skeleton and the CaCO$_3$ particles are leached to form pores. Thus, the thickness of the CNT/HDPE
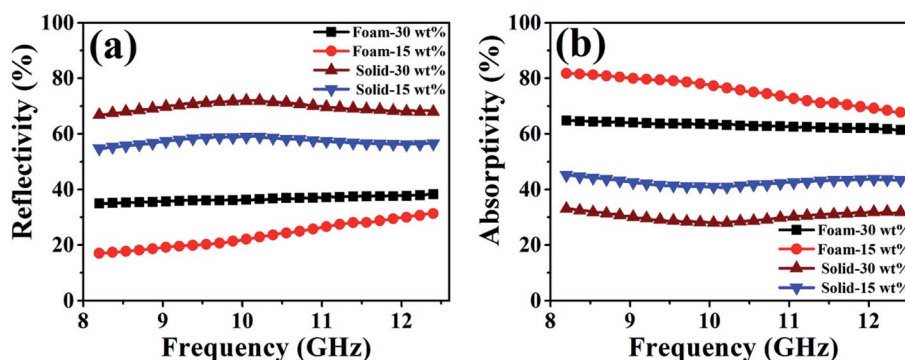

Fig. 6 Power reflectivity (a) and absorptivity (b) of the CNT/HDPE foam and solid composites at CNT loadings of 15 and 30 wt%.
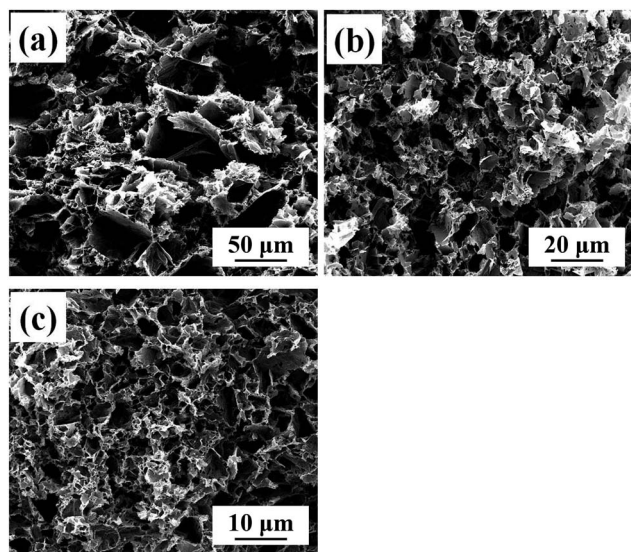
Fig. 7 SEM micrographs of the CNT/HDPE foam composites with various pore sizes: large (a), moderate (b), and small (c).
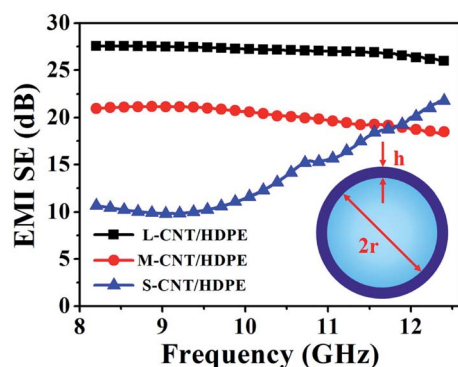

Fig. 8 EMI SE as a function of frequency for the CNT/HDPE foam composites with various pore sizes. The inset shows a representation of the assumed structure of the CNT/HDPE layer coated $CaCO_3$ particles.

a compression molding and salt-leaching method. The excluded volume effect caused by the foam structure promoted the local concentration of CNTs in the HDPE skeleton, thus leading to a lower percolation threshold and higher electrical conductivity for the CNT/HDPE foam composites compared to those of the solid composites. The superior electrical conductivity endowed the foam composites with a superior EMI shielding performance, with a specific EMI SE of about 2.2 times that of the solid composites. Moreover, the power reflectivity of the electromagnetic waves was significantly reduced from 55% for the solid composites to 17% for the foam composites. The integrated low reflectivity and high EMI SE are conducive to extending the application of the CNT/HDPE foam composites to microwave absorption.

Conflicts of interest

There are no conflicts to declare.

Acknowledgements

References

1 F. Shahzad, M. Alhabeb, C. B. Hatter, B. Anasori, S. Man Hong, C. M. Koo and Y. Gogotsi, *Science*, 2016, **353**, 1137–1140.

2 J. Liu, H. B. Zhang, R. Sun, Y. Liu, Z. Liu, A. Zhou and Z. Z. Yu, *Adv. Mater.*, 2017, **29**, 1702367.

3 W. L. Song, L. Z. Fan, M. S. Cao, M. M. Lu, C. Y. Wang, J. Wang, T. T. Chen, Y. Li, Z. L. Hou, J. Liu and Y. P. Sun, *J. Mater. Chem. A*, 2014, **2**, 5057–5064.

4 L. C. Jia, D. X. Yan, Y. Yang, D. Zhou, C. H. Cui, E. Bianco, J. Lou, R. Vajtai, B. Li, P. M. Ajayan and Z. M. Li, *Adv. Mater. Technol.*, 2017, **2**, 1700078.

5 Y. Chen, H. B. Zhang, Y. Yang, M. Wang, A. Cao and Z. Z. Yu, *Adv. Funct. Mater.*, 2016, **26**, 447–455.

6 L. C. Jia, D. X. Yan, C. H. Cui, X. Jiang, X. Ji and Z. M. Li, *J. Mater. Chem. C*, 2015, **3**, 9369–9378.

7 K. Zhang, H. O. Yu, Y. D. Shi, Y. F. Chen, J. B. Zeng, J. Guo, B. Wang, Z. Guo and M. Wang, *J. Mater. Chem. C*, 2017, **5**, 2807–2817.

8 M. H. Al-Saleh, W. H. Saadeh and U. Sundararaj, *Carbon*, 2013, **60**, 146–156.

9 S. T. Hsiao, C. C. M. Ma, H. W. Tien, W. H. Liao, Y. S. Wang, S. M. Li, C. Y. Yang, S. C. Lin and R. B. Yang, *ACS Appl. Mater. Interfaces*, 2015, **7**, 2817–2826.

10 L. C. Jia, Y. K. Li and D. X. Yan, *Carbon*, 2017, **121**, 267–273.

11 Q. F. Jing, J. Y. Law, L. P. Tan, V. V. Silberschmidt, L. Li and Z. L. Dong, *Composites, Part A*, 2015, **70**, 8–15.

skeleton should be proportional to the pore size. The greater thickness of the CNT/HDPE skeleton is beneficial for the formation of more perfect conductive networks in the final foam composites. Typically, the electrical conductivities of L-CNT/HDPE, M-CNT/HDPE and S-CNT/HDPE are 6.30 S m^{-1}, 0.98 S m^{-1} and 1.85×10^{-3} S m^{-1}, respectively. The higher electrical conductivity of L-CNT/HDPE contributes to its superior EMI SE. Moreover, it is noted that the EMI SE of S-CNT/HDPE strongly interacts with the frequency at higher frequencies. This can be attributed to its low electrical conductivity and large skin depth (Fig. S2†) (detailed calculations and explanation can be found in the ESI†).

4 Conclusions

CNT/HDPE foam composites with a high EMI SE (27.1 dB) and low density (0.26 g cm^{-3}) were easily fabricated using

12 L. C. Jia, M. Z. Li, D. X. Yan, C. H. Cui, H. Y. Wu and Z. M. Li, *J. Mater. Chem. C*, 2017, **5**, 8944–8951.

13 Y. Yang, M. C. Gupta, K. L. Dudley and R. W. Lawrence, *Nano Lett.*, 2005, **5**, 2131–2134.

14 J. Liu, H. B. Zhang, Y. Liu, Q. Wang, Z. Liu, Y. W. Mai and Z. Z. Yu, *Compos. Sci. Technol.*, 2017, **151**, 71–78.

15 C. H. Cui, D. X. Yan, H. Pang, L. C. Jia, X. Xu, S. Yang, J. Z. Xu and Z. M. Li, *Chem. Eng. J.*, 2017, **323**, 29–36.

16 Y. J. Chen, Y. Li, B. T. T. Chu, I. T. Kuo, M. Yip and N. Tai, *Composites, Part B*, 2015, **70**, 231–237.

17 D. X. Yan, P. G. Ren, H. Pang, Q. Fu, M. B. Yang and Z. M. Li, *J. Mater. Chem.*, 2012, **22**, 18772–18774.

18 J. Li, H. Liu, J. Guo, Z. Hu, Z. Wang, B. Wang, L. Liu, Y. Huang and Z. Guo, *J. Mater. Chem. C*, 2017, **5**, 1095–1105.

19 Z. Chen, C. Xu, C. Ma, W. Ren and H. M. Cheng, *Adv. Mater.*, 2013, **25**, 1296–1300.

20 B. Shen, Y. Li, W. Zhai and W. Zheng, *ACS Appl. Mater. Interfaces*, 2016, **8**, 8050–8057.

21 J. M. Thomassin, C. Jérôme, T. Pardoen, C. Bailly, I. Huynen and C. Detrembleur, *Mater. Sci. Eng., R*, 2013, **74**, 211–232.

22 J. Ling, W. Zhai, W. Feng, B. Shen, J. Zhang and W. g. Zheng, *ACS Appl. Mater. Interfaces*, 2013, **5**, 2677–2684.

23 B. Shen, W. Zhai, M. Tao, J. Ling and W. Zheng, *ACS Appl. Mater. Interfaces*, 2013, **5**, 11383–11391.

24 D. X. Yan, H. Pang, B. Li, R. Vajtai, L. Xu, P. G. Ren, J. H. Wang and Z. M. Li, *Adv. Funct. Mater.*, 2015, **25**, 559–566.

25 C. Li, G. Yang, H. Deng, K. Wang, Q. Zhang, F. Chen and Q. Fu, *Polym. Int.*, 2013, **62**, 1077–1084.

26 N. Athanasopoulos, A. Baltopoulos, M. Matzakou, A. Vavouliotis and V. Kostopoulos, *Polym. Compos.*, 2012, **33**, 1302–1312.

27 M. Antunes, M. Mudarra and J. I. Velasco, *Carbon*, 2011, **49**, 708–717.

28 A. Fletcher, M. C. Gupta, K. L. Dudley and E. Vedeler, *Compos. Sci. Technol.*, 2010, **70**, 953–958.

29 V. Eswaraiah, V. Sankaranarayanan and S. Ramaprabhu, *Macromol. Mater. Eng.*, 2011, **296**, 894–898.

30 J. M. Thomassin, C. Pagnoulle, L. Bednarz, I. Huynen, R. Jerome and C. Detrembleur, *J. Mater. Chem. C*, 2008, **18**, 792–796.

31 D. X. Yan, L. Xu, C. Chen, J. H. Tang, X. Ji and Z. M. Li, *Polym. Int.*, 2012, **61**, 1107–1114.

32 S. Kirkpatrick, *Rev. Mod. Phys.*, 1973, **45**, 574.

33 N. Inaba, K. Sato, S. Suzuki and T. Hashimoto, *Macromolecules*, 1986, **19**, 1690–1695.

34 I. Balberg, *Phys. Rev. Lett.*, 1987, **59**, 1305–1308.

35 Y. Chen, H. B. Zhang, Y. Yang, M. Wang, A. Cao and Z. Z. Yu, *Adv. Funct. Mater.*, 2016, **26**, 447–455.

36 L. C. Jia, D. X. Yan, C. H. Cui, X. Ji and Z. M. Li, *Macromol. Mater. Eng.*, 2016, **301**, 1232–1241.

37 Y. Yang, M. C. Gupta, K. L. Dudley and R. W. Lawrence, *Nano Lett.*, 2005, **5**, 2131–2134.

38 J. Ling, W. Zhai, W. Feng, B. Shen, J. Zhang and W. g. Zheng, *ACS Appl. Mater. Interfaces*, 2013, **5**, 2677–2684.

39 H. B. Zhang, Q. Yan, W. G. Zheng, Z. He and Z. Z. Yu, *ACS Appl. Mater. Interfaces*, 2011, **3**, 918–924.

40 Y. Li, X. Pei, B. Shen, W. Zhai, L. Zhang and W. Zheng, *RSC Adv.*, 2015, **5**, 24342–24351.

41 M. M. Bernal, M. Martin-Gallego, I. Molenberg, I. Huynen, M. A. L. Manchado and R. Verdejo, *RSC Adv.*, 2014, **4**, 7911–7918.

42 L. Monnereau, L. Urbanczyk, J. M. Thomassin, T. Pardoen, C. Bailly, I. Huynen, C. Jérôme and C. Detrembleur, *Polymer*, 2015, **59**, 117–123.

43 H. Wang, K. Zheng, X. Zhang, X. Ding, Z. Zhang, C. Bao, L. Guo, L. Chen and X. Tian, *Compos. Sci. Technol.*, 2016, **125**, 22–29.

44 J. M. Thomassin, D. Vuluga, M. Alexandre, C. Jérôme, I. Molenberg, I. Huynen and C. Detrembleur, *Polymer*, 2012, **53**, 169–174.